J. Fluid Mech. (2024), *vol*. 1000, A50, doi:10.1017/jfm.2024.1053

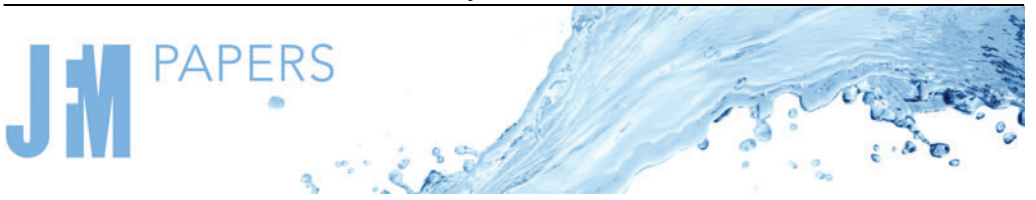

Energetics of particle-size segregation

Tomás Trewhela[1],† **and Hugo N. Ulloa**[2],†

[1]Facultad de Ingeniería y Ciencias, Universidad Adolfo Ibañez, Av. Padre Hurtado 750, 2562340 Viña del Mar, Chile

[2]Department of Earth and Environmental Science, University of Pennsylvania, Philadelphia, PA 19104-6316, USA

(Received 13 June 2024; revised 30 September 2024; accepted 28 October 2024)

We introduce a continuum framework for the energetics of particle-size segregation in bidisperse granular flows. Building on continuum segregation equations and a recent segregation flux model, the proposed framework offers general analytical expressions to study the physics of granular flows from a mechanical energy perspective. We demonstrate the framework's applicability by examining the energetics of shear-driven granular flows. Numerical experiments with varying frictional coefficients and particle-size ratios reveal two distinct phases in the energetics, marked by the separate onset of particle segregation and diffusive remixing. Furthermore, our numerical simulations alongside previous experimental results show that the bulk Richardson number Ri, defined as the potential energy to kinetic energy ratio at steady state, follows the scaling relationship $Ri \equiv \hat{E}_{gp}^{(s)}/\hat{E}_{k}^{(s)} \propto Pe_{sr}^{-1/2}$ for $0.1 \leq Ri \leq 10^3$ and $10^{-4} \leq Pe_{sr} \leq 300$, the segregation–rheology Péclet number. Finally, we present a Péclet-number-dependent theoretical expression for the degree of mixing (or segregation), validated by the compiled numerical and experimental dataset. Our findings hint that the bulk segregation–mixing state can be predicted and controlled using the segregation Péclet number Pe and Pe_{sr}, both determined from known system parameters, providing an instrumental tool for engineering and geophysical applications.

Key words: dry granular material, granular mixing, sediment transport

1. Introduction

Granular materials segregate and mix as they flow (Ottino & Khakhar 2000; Gray 2018; Umbanhowar, Lueptow & Ottino 2019). Although no general agreement exists on the determining drivers, relative motion between particles of differing sizes comprising a granular bulk is essential for segregation, occurring when available mechanical

† Email addresses for correspondence: tomas.trewhela@uai.cl, ulloa@sas.upenn.edu

energy – sourced from external forcing or gravity – is transformed into kinetic energy. However, how does the available energy partition between segregation, mixing and interparticle friction within the granular bulk? Addressing this question is crucial not only for understanding granular flow dynamics but also for optimising engineering processes aiming at transporting, segregating or mixing polydisperse materials.

Research on the energetics of polydisperse granular flows remains limited. Most of the studies have focused on characterising the energy dissipated by friction (e.g. Hurley & Andrade 2015; Pereira & Cleary 2017; Jiang *et al.* 2018; Varela-Rosales *et al.* 2023), and only a few have connected energy characteristics with granular flow regimes. Using discrete element simulations, Sun, Jin & Zhou (2013) found that the effective friction coefficient in sheared bidisperse granular flows is inversely proportional to the ratio of elastic to kinetic energy, and emphasised that energetics studies could bridge the mechanics from quasi-static to rapid flow regimes. Despite these insights, a comprehensive understanding of how mechanical energy transforms and relates to segregation–mixing states in flowing granular mixtures is still lacking.

The segregation–mixing states are intuitively related to the segregation Péclet number Pe, defined as the ratio between segregation and diffusive fluxes in dense granular flows (Gray & Chugunov 2006; Trewhela 2024). While large Pe values are associated with enhanced segregation, small Pe results in more mixed states with diffusion acting as the main mixing driver. Such determinant roles of segregation and diffusive remixing, hence of Pe, have been found in theory (Gray & Chugunov 2006), and in both laboratory (Wiederseiner *et al.* 2011; Maguire *et al.* 2024) and numerical (e.g. Thornton *et al.* 2012; Fan *et al.* 2014) experiments. However, a clear-cut general relationship between the final state for segregation (or mixing) and Pe is missing. An additional non-dimensional parameter, the segregation–rheology Péclet number Pe_{sr}, can be introduced to characterise the coupling between segregation and rheology. This recently introduced definition proposes a balance between segregation and momentum transfer within the granular bulk and its different particle species (Trewhela 2024), yet the role of Pe_{sr} on mixing and the species energy distribution remains unclear. Nonetheless, the state of mixing of materials that segregate can also be explored in terms of other fundamental parameters. One of them is the bulk Richardson number Ri, balancing the competition between the stabilising effect of buoyancy and the destabilising impact of inertia in mixing stratified systems (e.g. Caulfield 2021). In addition to Ri, the 'degree of mixing' $\mathscr{M}_\phi$ or 'degree of segregation' $\mathscr{S}_\phi = 1 - \mathscr{M}_\phi$, determined from the spatial variance of particles distribution, provide a concise quantitative measure of how mixed or segregated polydisperse systems are at any given time. These parameters, while not commonly utilised to characterise segregation–mixing states of granular flows, have shown effectiveness in describing stratified and convective fluid flows dynamics (Jha, Cueto-Felgueroso & Juanes 2011; Caulfield 2021; Ulloa & Letelier 2022). As such, we propose that they also serve to characterise granular flows.

Combining segregation theory (Gray 2018) with laboratory experiments, the Trewhela, Ancey & Gray (2021*a*) scaling law for particle-size segregation provides robust predictions for segregation in dense granular flows from various physical parameters. Yet advancing the modelling of granular flows in complex configurations requires characterising the energy source, and how this energy partitions and transforms within and by the granular bulk. An energetics framework for granular flows is therefore instrumental in quantifying how much of the available energy leads to particles' motion, segregation, mixing and irreversible dissipation due to friction.

This paper introduces a new continuum framework for characterising particle-size segregation and mixing from an energetics perspective. In § 2, we present the convection–diffusion model for particle-size segregation based on continuum–mixture theory (Gray 2018). Building on this and recent scaling law for segregation (Trewhela *et al.* 2021*a*), we derive the energetics for non-cohesive, inelastic, bidisperse particle flows in § 3. In § 4, we illustrate the framework's applicability by studying the energetics for shear-driven, bidisperse granular flows, revealing a new scaling relationship between the ratio of the bulk Richardson number and the segregation–rheology Péclet number. Finally, we derive a Péclet-number-dependent analytical expression for the degree of mixing and segregation of the granular flow – validated by numerical and laboratory experiments – that offers potential applications for controlling industrial processes and interpreting geophysical phenomena.

2. Theoretical framework

2.1. *Bidisperse particle-size segregation equations*

We consider non-cohesive granular media of bidisperse, rigid spherical particles – of differing small d_s and large $d_l > d_s$ diameters, but uniform density ρ_* – within a fixed volume V. The mass of the mixture is $M = M_l + M_s$, with $M_s = \rho_* n_s (\pi/6) d_s^3$ and $M_l = \rho_* n_l (\pi/6) d_l^3$ the masses of the small n_s particles and the large n_l particles, respectively. The solids volume fraction Φ is then determined by the ratio between M and the reference mass $M_* = \rho_* V$, so $\Phi = \Phi_l + \Phi_s$. In dynamic systems, each concentration Φ_ν ($\nu \in \{s, l\}$) is, in principle, space- and time-dependent. However, the concentration Φ usually varies little in most dense granular flows. By assuming Φ to be constant, we can express each particle-size concentration in terms of its corresponding species concentration, $\phi_s = \Phi_s/\Phi$ and $\phi_l = \Phi_l/\Phi$. Thus $\phi_s + \phi_l = 1$ establishes the inherent mass conservation law for the granular system.

The bidisperse granular material can be treated as a continuum medium, for which mixture theory applied to the granular bulk yields the convective–diffusive equations for segregation,

$$\frac{\partial \phi_s}{\partial t} + \boldsymbol{\nabla} \cdot (\phi_s \boldsymbol{u}) + \boldsymbol{\nabla} \cdot \left(f_{sl} \phi_s \phi_l \frac{\boldsymbol{g}}{|\boldsymbol{g}|} \right) = \boldsymbol{\nabla} \cdot (\mathcal{D}_{sl} \boldsymbol{\nabla} \phi_s), \tag{2.1a}$$

$$\frac{\partial \phi_l}{\partial t} + \boldsymbol{\nabla} \cdot (\phi_l \boldsymbol{u}) - \boldsymbol{\nabla} \cdot \left(f_{sl} \phi_s \phi_l \frac{\boldsymbol{g}}{|\boldsymbol{g}|} \right) = \boldsymbol{\nabla} \cdot (\mathcal{D}_{sl} \boldsymbol{\nabla} \phi_l), \tag{2.1b}$$

where $\boldsymbol{u}$ is the divergence-free granular bulk velocity, $\mathcal{D}_{sl}$ is the particle diffusivity, and $f_{sl}\phi_s\phi_l \boldsymbol{g}/|\boldsymbol{g}|$ characterises the segregation flux, with f_{sl} the particle-size segregation velocity magnitude (Trewhela *et al.* 2021*a*). The gravitational norm vector $\boldsymbol{g}/|\boldsymbol{g}|$ is included to confer a direction to size segregation, determined by the gravity-driven kinetic sieving and squeeze expulsion mechanisms (Gray 2018). The functional form of f_{sl} has been proposed to be quadratic or cubic, symmetrical or asymmetrical (Gajjar & Gray 2014; Umbanhowar *et al.* 2019). Recent scaling laws have aimed to parametrise f_{sl} in terms of physical quantities, such as pressure p, shear rate $\dot{\gamma}$, local particle concentrations ϕ_s, and particle diameter d. With that goal, Trewhela *et al.* (2021*a*) proposed that the segregation velocity magnitude f_{sl} could be described as

$$f_{sl} = \left(\frac{\mathcal{B} \rho_* g \dot{\gamma} \bar{d}^2}{p} \right) [(R_d - 1) + \mathcal{E}(1 - \phi_s)(R_d - 1)^2], \tag{2.2}$$

$$\mu_1 = 0.342, \quad \mu_2 = 0.557, \quad I_0 = 0.069, \quad \alpha = 1.9, \quad \mu_\infty = 0.05, \quad I_1 = 0.005, \quad A = 1.565 \times 10^4,$$
$$d_l = 143\,\mu\text{m}, \quad \rho_* = 2500\,\text{kg}\,\text{m}^{-3}, \quad \Phi = 0.6, \quad p_0 = 300\,\text{Pa}, \quad u_0 = 0.2\,\text{m}\,\text{s}^{-1}, \quad \chi_\mu = 0.0075,$$
$$\mathcal{A} = 0.108, \quad \mathcal{B} = 0.374, \quad \mathcal{E} = 2.096$$

Table 1. Parameters used in this work: frictional parameters μ_1, μ_2 and I_0 for the $\mu(I)$-rheology (Jop *et al.* 2006); coefficient μ_∞ with the fitting parameters α, I_1 and A for the partial regularisation of the $\mu(I)$-rheology, measured by Barker & Gray (2017) for $d_l = 143\,\mu$m glass beads; the grains' intrinsic density ρ_*; the solids volume fraction Φ; the specific values for pressure p_0 and velocity u_0 at the wall; and the frictional asymmetry coefficient χ_μ (Trewhela 2024). Finally, we give the constants for diffusivity $\mathcal{A}$ (Utter & Behringer 2004) and segregation $\mathcal{B}$, $\mathcal{E}$ (Trewhela *et al.* 2021*a*).

where $\mathcal{B} = 0.374$ and $\mathcal{E} = 2.096$ are empirical constants, $\bar{d} = \phi_s d_s + \phi_l d_l$ denotes the particles' concentration-averaged diameter, and $R_d = d_l/d_s$ defines the particles' size ratio. Merging the above expressions for $\bar{d}$ and R_d, the concentration-averaged diameter can be expressed as $\bar{d} = (1 - \chi_d \phi_s) R_d d_s$, which captures the asymmetric behaviour of size segregation by defining $\chi_d = (R_d - 1)/R_d$ as the asymmetry coefficient (Gajjar & Gray 2014; van der Vaart *et al.* 2015; Trewhela 2024). Note that the function (2.2) is not particular or case-dependent; it describes the segregation velocity for small and large particles at variable concentrations ϕ_s and $\phi_l = (1 - \phi_s)$, respectively, and it also compiles a comprehensive set of experimental and numerical results that hints at its dependence with pressure p, shear rate $\dot{\gamma}$ and size ratio R_d (Golick & Daniels 2009; Thornton *et al.* 2012; Fry *et al.* 2018; Chassagne *et al.* 2020; Trewhela, Gray & Ancey 2021*b*; Tripathi *et al.* 2021).

From the definition of Φ_ν, (2.1*a*) can be expressed directly as

$$\frac{\partial \Phi_\nu}{\partial t} + \boldsymbol{\nabla} \cdot (\Phi_\nu \boldsymbol{u}) + \boldsymbol{\nabla} \cdot \boldsymbol{F}_{\Phi_\nu} = \boldsymbol{\nabla} \cdot (\mathcal{D}_{sl} \boldsymbol{\nabla} \Phi_\nu), \tag{2.3}$$

where the segregation flux $\boldsymbol{F}_{\Phi_\nu}$ for the ν-particle species is defined as

$$\boldsymbol{F}_{\Phi_\nu} = \begin{cases} +f_{sl} \Phi_s [1 - \phi_s] \dfrac{\boldsymbol{g}}{|\boldsymbol{g}|} & \text{for } \nu = s, \\ -f_{sl} \Phi_l [1 - \phi_l] \dfrac{\boldsymbol{g}}{|\boldsymbol{g}|} & \text{for } \nu = l, \end{cases} \tag{2.4}$$

whereas the particles' diffusivity $\mathcal{D}_{sl} = \mathcal{A} \dot{\gamma} \bar{d}^2$ (Utter & Behringer 2004) is responsible for diffusive remixing and controls the final segregation state, with $\mathcal{A} = 0.108$ an empirical constant (table 1).

3. Energetics for the segregation of the ν-particle species

Assuming inelastic grains, the potential energy for the ν-particle species in the volume V of domain Ω is only determined by the gravitational component,

$$E_{gp}^{(\nu)} = \int_\Omega \rho_* g z \Phi_\nu \, \mathrm{d}V, \tag{3.1}$$

with $\mathscr{E}_{gp}^{(\nu)}(t, \boldsymbol{x}) = \rho_* g z \, \Phi_\nu(t, \boldsymbol{x})$ the gravitational potential energy (GPE) density, and z the vertical coordinate pointing upwards. Likewise, we define the kinetic energy (KE) of the

ν-particle species within the volume V as

$$E_k^{(\nu)} = \frac{1}{2}\int_{\Omega} \rho_* \Phi_\nu \, |\boldsymbol{u}|^2 \, \mathrm{d}V, \tag{3.2}$$

with $\mathscr{E}_k^{(\nu)}(t, \boldsymbol{x}) = \frac{1}{2}\rho_* \, \Phi_\nu(t, \boldsymbol{x}) \, |\boldsymbol{u}(t, \boldsymbol{x})|^2$ the KE density.

3.1. *Energetics for the GPE*

Building upon the convective–diffusive equations for ϕ_ν in (2.3), the evolution equation for the GPE density of the ν-particle species is given by

$$\frac{\partial \mathscr{E}_{gp}^{(\nu)}}{\partial t} = \rho_* g z[-\boldsymbol{\nabla}\cdot(\Phi_\nu \boldsymbol{u}) - \boldsymbol{\nabla}\cdot\boldsymbol{F}_{\Phi_\nu} + \boldsymbol{\nabla}\cdot(\mathcal{D}_{sl}\,\boldsymbol{\nabla}\Phi_\nu)]. \tag{3.3}$$

Utilising vector identities and the divergence theorem, the evolution equation for the GPE in the volume V unfolds as

$$\begin{aligned}\frac{\mathrm{d}E_{gp}^{(\nu)}}{\mathrm{d}t} = &\underbrace{-\oint_{\partial\Omega} \rho_* g z[\Phi_\nu \boldsymbol{u} + \boldsymbol{F}_{\Phi_\nu} - \mathcal{D}_{sl}\,\boldsymbol{\nabla}\Phi_\nu]\cdot\hat{\boldsymbol{n}}\,\mathrm{d}S}_{\Sigma_{gp}^{(\nu)}} \\ &+ \underbrace{\int_{\Omega} \rho_* g \Phi_\nu w \,\mathrm{d}V}_{\Psi_c^{(\nu)}} + \underbrace{\int_{\Omega} \rho_* g \boldsymbol{F}_{\Phi_\nu}\cdot\hat{\boldsymbol{k}}\,\mathrm{d}V}_{\Psi_{gps}^{(\nu)}} - \underbrace{\int_{\Omega} \rho_* g \mathcal{D}_{sl}\frac{\partial \Phi_\nu}{\partial z}\,\mathrm{d}V}_{\Psi_{gpd}^{(\nu)}}.\end{aligned} \tag{3.4}$$

Therefore, the rate of change of $E_{gp}^{(\nu)}$ is determined by four main energetics that characterise the injection/extraction, transformation and dissipation of GPE due to redistribution and dynamics of the ν-particle species.

The first term on the right-hand side of (3.4) quantifies the energetics associated with the net boundary energy flux $\Sigma_{gp}^{(\nu)}$, which integrates fluxes resulting from the advection, segregation and diffusion of particles at the boundary of the granular bulk. In the case of granular systems with adiabatic boundaries, $\Sigma_{gp}^{(\nu)}$ equals 0. Conversely, when granular flows experience mass exchange at the boundaries, there is a resultant gain or loss of GPE in which $\Sigma_{gp}^{(\nu)} > 0$ or $\Sigma_{gp}^{(\nu)} < 0$, respectively. The second term $\Psi_c^{(\nu)}$ quantifies the rate of change of $E_{gp}^{(\nu)}$ due to the energetics associated with vertical convective flows that redistribute particles within the moving granular mixture. Whereas the third $\Psi_{gps}^{(\nu)}$ and fourth $\Psi_{gpd}^{(\nu)}$ terms characterise the rate of change of $E_{gp}^{(\nu)}$ owing to segregation and diffusion of particles in the vertical direction, respectively. The nature of the last two energetics reflects competitive dynamics, where both may contribute to increase or decrease the GPE, depending on the ν-particle species involved. For instance, in a gravity-driven granular current, larger particles ($\nu = l$) tend to segregate to the free surface, thereby raising the GPE at a rate $\Psi_{gps}^{(l)}$. However, the energetics associated with the diffusion of large particles $\Psi_{gpd}^{(l)}$ acts to counterbalance this by hindering complete segregation, hence reducing the maximum attainable GPE. Conversely, in the same granular flow, smaller particles ($\nu = s$) tend to segregate (percolate) to the base due to kinetic sieving, resulting in an energy flux that decreases GPE at a rate $\Psi_{gps}^{(s)}$. In this case, the vertical diffusion of small particles

works to raise GPE at a rate $\Psi_{gpd}^{(s)}$, opposing the system's tendency towards its minimum GPE.

3.2. *Energetics for the KE*

The evolution equation for the KE density is derived from

$$\frac{\partial \mathscr{E}_k^{(\nu)}}{\partial t} = \rho_* \frac{1}{2} |\boldsymbol{u}|^2 \frac{\partial \Phi_\nu}{\partial t} + \rho_* \Phi_\nu \boldsymbol{u} \cdot \frac{\partial \boldsymbol{u}}{\partial t}, \tag{3.5}$$

and the continuum linear momentum equation for the particles mixture,

$$\rho_* \Phi \left[\frac{\partial \boldsymbol{u}}{\partial t} + \nabla \left(\frac{1}{2} |\boldsymbol{u}|^2 \right) \right] = \nabla \cdot \boldsymbol{T} + \rho_* \Phi \boldsymbol{g}. \tag{3.6}$$

The stress tensor can be decomposed into $\boldsymbol{T} = \boldsymbol{\tau} - p\boldsymbol{1}$, with p the pressure multiplying the tensor identity, and $\boldsymbol{\tau}$ the deviatoric shear stress. Consequently, from (2.3) and (3.6), the evolution equation of $\mathscr{E}_k^{(\nu)}(t, \boldsymbol{x})$ is given by

$$\begin{aligned} \frac{\partial \mathscr{E}_k^{(\nu)}}{\partial t} = {} & \frac{1}{2} \rho_* |\boldsymbol{u}|^2 \{ -\nabla \cdot (\Phi_\nu \boldsymbol{u}) - \nabla \cdot \boldsymbol{F}_{\Phi_{sl}} + \nabla \cdot (\mathcal{D}_{sl} \nabla \Phi_\nu) \} \\ & + \boldsymbol{u} \cdot \left\{ -\rho_* \Phi_\nu \nabla \left(\frac{1}{2} |\boldsymbol{u}|^2 \right) + \phi_\nu \nabla \cdot \boldsymbol{T} + \rho_* \Phi_\nu \boldsymbol{g} \right\}. \end{aligned} \tag{3.7}$$

Integrating (3.7) in the volume V, the evolution equation for the KE is given by

$$\begin{aligned} \frac{\mathrm{d}E_k^{(\nu)}}{\mathrm{d}t} = {} & \underbrace{- \int_{\partial\Omega} \left[\frac{\rho_*}{2} |\boldsymbol{u}|^2 (\Phi_\nu \boldsymbol{u} + \boldsymbol{F}_{\Phi_\nu} - \mathcal{D}_{sl} \nabla \Phi_\nu) - (\phi_\nu \boldsymbol{u} \cdot \boldsymbol{T}) \right] \cdot \hat{\boldsymbol{n}} \, \mathrm{d}S}_{\Sigma_k^{(\nu)}} \\ & + \underbrace{\int_\Omega \boldsymbol{F}_{\Phi_\nu} \cdot \nabla \left(\frac{\rho_*}{2} |\boldsymbol{u}|^2 \right) \mathrm{d}V}_{\Psi_{ks}^{(\nu)}} - \underbrace{\int_\Omega \mathcal{D}_{sl} \nabla \Phi_\nu \cdot \nabla \left(\frac{\rho_*}{2} |\boldsymbol{u}|^2 \right) \mathrm{d}V}_{\Psi_{kd}^{(\nu)}} \\ & - \Psi_c^{(\nu)} - \underbrace{\int_\Omega \nabla (\phi_\nu \boldsymbol{u}) : \boldsymbol{T} \, \mathrm{d}V}_{\Psi_\mu^{(\nu)}}. \end{aligned} \tag{3.8}$$

Therefore, the rate of change of $E_k^{(\nu)}$ is determined by five main energetics, which characterise the injection/extraction, transformation and dissipation of KE due to redistribution and dynamics of the ν-particle species.

The first term $\Sigma_k^{(\nu)}$ on the right-hand side of (3.8) quantifies the energetics associated with the net boundary energy flux, which integrates fluxes resulting from advection, segregation, diffusion and interparticle friction. For granular systems with adiabatic and frictionless boundaries, $\Sigma_k^{(\nu)}$ equals zero. Otherwise, boundaries act as surface areas through which energy is either injected or extracted by friction, being shear-driven granular flows, a canonical example of a system wherein $\Sigma_k^{(\nu)}$ is positive, thereby contributing to the sourcing of KE.

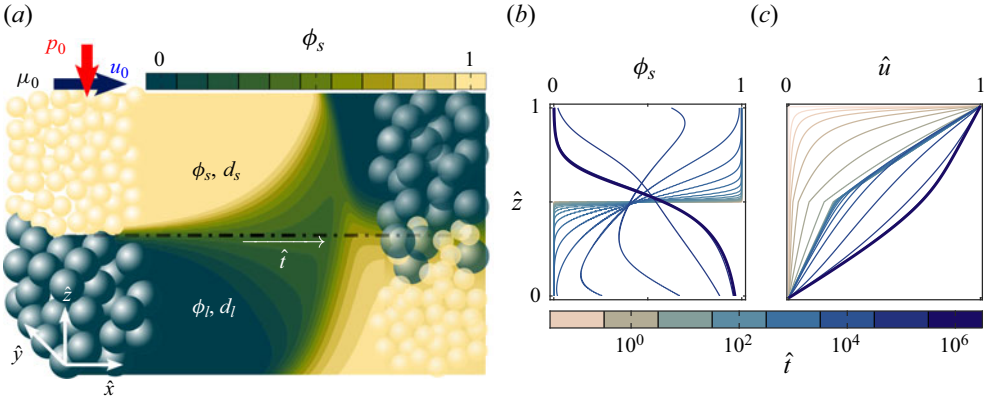

Figure 1. (*a*) Schematic of the case study and an example of the numerical simulations. (*b*,*c*) Temporal evolutions of the small-particle species concentration $\phi_s(\hat{t}, \hat{z})$ and velocity profile $\hat{u}(\hat{t}, \hat{z})$ for $R_d = 2.5$, $\mu_0 = 0.5$.

The second term $\Psi_{ks}^{(\nu)}$ on the right-hand side of (3.8) quantifies the energetics of $E_k^{(\nu)}$ due to ν-particle species segregation within the moving granular bulk. Since $\boldsymbol{F}_{\Phi_\nu}$ is parallel to the gravitational acceleration vector $\boldsymbol{g}/|\boldsymbol{g}|$, commonly characterised by $-\hat{\boldsymbol{z}}$ (see figure 1), spatial gradients of $\rho_* |\boldsymbol{u}|^2/2$ in directions perpendicular to $\boldsymbol{g}/|\boldsymbol{g}|$ do not contribute to $\Psi_{ks}^{(\nu)}$. As an example, let us consider a bidisperse granular flow driven by shear stress exerted at the granular bulk's surface, moving at a speed u_0. The resulting velocity profile increases linearly with height z, i.e. $\boldsymbol{u} = u_0(z/h)\,\hat{\boldsymbol{x}}$, with h the sheared layer. In this context, the energetics of segregation simplifies to $\Psi_{ks}^{(\nu)} = \int_\Omega \boldsymbol{F}_{\Phi_\nu} \cdot (\rho_* u\, \partial u/\partial z)\,\hat{\boldsymbol{z}}\,\mathrm{d}V$. Interestingly, the sign of $\Psi_{ks}^{(\nu)}$ depends on the ν-particle species. If $u(\partial u/\partial z) > 0$, then the KE flux owing to segregation is positive for large particles ($\nu = l$): $\Psi_{ks}^{(l)} = \int_\Omega f_{sl}\Phi_l[1-\phi_l](\rho_* u\, \partial u/\partial z)\,\mathrm{d}V > 0$. In this scenario, large particle species segregate into upper regions characterised by a granular flow with higher inertia and density of KE. Conversely, for the case of small particles ($\nu = s$), the KE flux owing to segregation is negative: $\Psi_{ks}^{(s)} = -\int_\Omega f_{sl}\Phi_s[1-\phi_s](\rho_* u\, \partial u/\partial z)\,\mathrm{d}V < 0$. Here, small-particle species segregate into deeper regions characterised by a granular flow with a lower inertia and density of KE, resulting in a global loss of their KE.

The third $\Psi_{kd}^{(\nu)}$ and fourth $\Psi_c^{(\nu)}$ terms on the right-hand side of (3.8) correspond to the energetics that quantify the rate of change of $E_k^{(\nu)}$ owing to diffusion and convective flows that redistribute ν-particle species vertically within the granular matrix. We remark that the sign of the energy flux due to diffusion $\Psi_{kd}^{(\nu)}$ also depends on the ν-particle species. To illustrate this, we consider the same bidisperse granular flow discussed earlier, which allows us to simplify the term to $\Psi_{kd}^{(\nu)} = \int_\Omega \mathcal{D}_{sl}(\partial\Phi_\nu/\partial z)(\rho_* u\, \partial u/\partial z)\,\mathrm{d}V$. Assuming that $u(\partial u/\partial z) > 0$, the actual sign of $\Psi_{kd}^{(\nu)}$ is determined by the gradient $\partial\Phi_\nu/\partial z$, which may also change over time, as shown later in figure 1(*b*) and evaluated in § 4. Finally, the term $\Psi_\mu^{(\nu)}$ is general and characterises the energetics associated with the irreversible loss of KE due to interparticle friction, commonly referred to as the KE dissipation rate. Note that a closed-form mathematical expression for $\Psi_\mu^{(\nu)}$ requires a constitutive relationship between the stress tensor $\boldsymbol{T}$ and the granular mixture rheology. In this direction, the proposed

framework is flexible enough to allow the usage of local or non-local rheological models (Kamrin *et al.* 2024), without loss of generality.

4. Application: shear-driven granular flow

The framework introduced in § 3 allows us to investigate granular flows from an energy perspective. We illustrate its applicability by examining the energetics of sheared granular flows undergoing segregation and mixing dynamics. For such a configuration, we must have a constitutive law relating stresses and the granular mixture rheology to determine the energy injection and dissipation resulting from particles' friction, $\Psi_\mu^{(\nu)}$, which are defined next.

4.1. *Stress tensor and $\mu(I)$-rheology for bidisperse granular mixtures*

To calculate $\Sigma_k^{(\nu)}$ and $\Psi_\mu^{(\nu)}$ in (3.8), the stress tensor $\boldsymbol{T}$ needs to be described thoroughly. A widely used relationship to do so is the $\mu(I)$-rheology, that relates the shear τ and normal p stresses through a Coulombic relation $\tau = \mu(I)\, p$. Embedded within this definition, the frictional coefficient $\mu(I)$ is found to be dependent on the inertial number (e.g. MiDi 2004)

$$I = \frac{\dot{\gamma}\bar{d}}{\sqrt{p/\rho^*}}. \tag{4.1}$$

The frictional coefficient is obtained by fitting the empirically determined function $\mu(I) = \mu_1 + (\mu_2 - \mu_1)/(I_0/I + 1)$, where μ_1 and μ_2 are the static and dynamic frictional coefficients, respectively (Jop, Forterre & Pouliquen 2006). These two coefficients, alongside the material parameter I_0, correspond to the experimental parameters that define the $\mu(I)$-rheology. However, the above relationship for $\mu(I)$ is ill-posed. Barker & Gray (2017) partially regularised the $\mu(I)$ definition with the extended relationship

$$\mu(I) = \begin{cases} \sqrt{\alpha/\log(A/I)}, & \text{for } I \leq I_1, \\ \dfrac{\mu_1 I_0 + \mu_2 I + \mu_\infty I^2}{I + I_0}, & \text{for } I > I_1, \end{cases} \tag{4.2}$$

where μ_∞, α and I_1 are material-dependent coefficients. The two latter parameters with A serve as fitting constants for the partially regularised $\mu(I)$-rheology, which guarantees continuity of (4.2). For this work, the values for all these parameters and constants defining the $\mu(I)$-rheology are presented in table 1.

To include bidispersity effects in the bulk's frictional response, we define a concentration-averaged frictional coefficient $\bar{\mu} = \mu_s\phi_s + \mu_l\phi_l = (1 - \chi_\mu\phi_s)R_\mu\mu_s$, where μ_ν denotes the frictional coefficient for the ν species, and $R_\mu = \mu_l/\mu_s$ is a ratio that defines the asymmetry parameter $\chi_\mu = (R_\mu - 1)/R_\mu$ (Trewhela 2024) (see table 1). From the above definitions, the stress tensor components are given by

$$T_{ij} = \begin{cases} \bar{\mu}(I)\, p - p, & \text{for } i = j, \\ \bar{\mu}(I) p, & \text{for } i \neq j, \end{cases} \quad \text{with } i, j = \{x, z\}, \tag{4.3}$$

which are naturally averaged over the concentrations of particle species.

4.2. *Energetics of a sheared bidisperse granular layer*

As a case study, we consider a bidisperse granular bulk of depth h sustaining shear exerted by a top plate imposing a uniform normal pressure distribution $p = p_0$ and moving at a constant velocity u_0 in the streamwise x-direction (figure 1*a*). Based on the rheological model in § 4.1, the pressure p_0, velocity u_0 and frictional coefficient μ_0 set a shear $\tau_{xz} = \tau_0 = p_0\mu_0$ (table 1) at the top boundary. In contrast, the granular material in contact with the motionless bottom does not slip or roll. Under these conditions, the granular system develops a zero-gravity shear flow, which, for simplicity, is treated as two-dimensional and periodic in the x-direction. As a result, the sheared layer depends on the upper boundary condition (John Soundar Jerome & Di Pierro 2018)

$$h = \left(\frac{\mu_0}{\mu_1} - 1\right)\frac{p_0}{\rho_* g \Phi}. \tag{4.4}$$

The top and bottom boundaries are closed, so fluxes across them are null. Without loss of generality, we examine the momentum–segregation equations of the small-particle species, i.e. $\nu = s$, which, in non-dimensional form, are given by

$$\frac{\partial \hat{u}}{\partial \hat{t}} = \frac{\partial}{\partial \hat{z}}([1 - \chi_\mu \phi_s] R_\mu \mu_s \hat{p}), \quad \frac{\partial \phi_s}{\partial \hat{t}} = \frac{\partial}{\partial \hat{z}}\left(\hat{f}_{sl}\phi_s[1-\phi_s] + \hat{\mathcal{D}}_{sl}\frac{\partial \phi_s}{\partial \hat{z}}\right), \tag{4.5a,b}$$

where $\hat{u} = u/u_0, \hat{p} = p/p_0, \hat{z} = z/h, \hat{t} = t/(h/u_0), \hat{f}_{sl} = f_{sl}/u_0$ and $\hat{\mathcal{D}}_{sl} = \mathcal{D}_{sl}/(u_0 h)$ denote the non-dimensional variables (Trewhela 2024). From (4.5*a*,*b*) and considering the energy scale per unit area $\Phi\rho_* g h^2$, the evolution equation for the non-dimensional GPE, $\hat{E}_{gp}^{(s)} = \int_0^1 \phi_s \hat{z}\,\mathrm{d}\hat{z}$, reduces to

$$\frac{\mathrm{d}\hat{E}_{gp}^{(s)}}{\mathrm{d}t} = \underbrace{\int_0^1 -\hat{f}_{sl}\phi_s[1-\phi_s]\,\mathrm{d}\hat{z}}_{\hat{\Psi}_{gps}^{(s)}} - \underbrace{\int_0^1 \hat{\mathcal{D}}_{sl}\frac{\partial \phi_s}{\partial \hat{z}}\,\mathrm{d}\hat{z}}_{\hat{\Psi}_{gpd}^{(s)}}. \tag{4.6}$$

Likewise, considering the same energy scale, the evolution equation for the non-dimensional KE, $\hat{E}_k^{(s)} = \frac{1}{2}Fr^2\int_0^1 \hat{u}^2\,\mathrm{d}\hat{z}$, simplifies to

$$\frac{\mathrm{d}\hat{E}_k^{(s)}}{\mathrm{d}\hat{t}} = \underbrace{Fr^2\,(\hat{u}[1-\chi_\mu\phi_s]R_\mu\mu_s\hat{p})|_{\hat{z}=1}}_{\hat{\Sigma}_k^{(s)}} - \underbrace{Fr^2\int_0^1 [1-\chi_\mu\phi_s]R_\mu\mu_s\hat{p}\,\frac{\partial \hat{u}}{\partial \hat{z}}\,\mathrm{d}\hat{z}}_{\hat{\Psi}_\mu^{(s)}}, \tag{4.7}$$

where $Fr = u_0/\sqrt{gh}$ is the Froude number of the bulk granular flow. The energetics $\hat{\Sigma}_k^{(s)}$ and $\Psi_\mu^{(s)}$ are positive definite and determine the rate of kinetic (mechanical) energy production due to surface shear and KE dissipation owing to friction, respectively. In contrast, the energetics $\hat{\Psi}_{gps}^{(s)}$ and $\hat{\Psi}_{gpd}^{(s)}$ quantify the transformation rate of potential (mechanical) energy due to vertical segregation and diffusion of particles, respectively; their signs are not defined *a priori*. The energy pathways controlled by the processes responsible for transforming the mechanical energy – i.e. segregation, particle diffusion and friction – are unknown and investigated next.

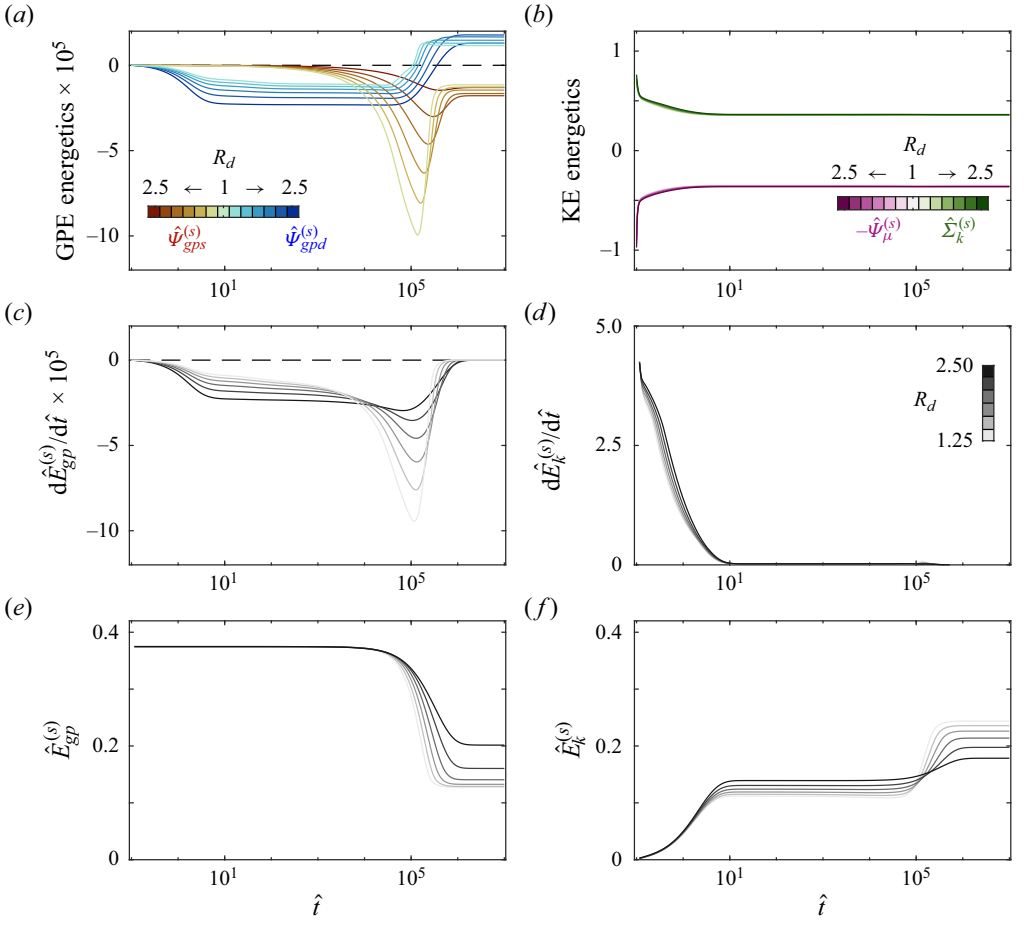

Figure 2. Numerical results for $\mu_0 \times R_d = \{0.8\} \times \{1.25, 1.5, 1.75, 2.0, 2.25, 2.5\}$. (*a*) Energetics of GPE, $\hat{\Psi}^{(s)}_{gps}$ and $\hat{\Psi}^{(s)}_{gpd}$ versus time $\hat{t}$. (*b*) Energetics of KE, $\hat{\Sigma}^{(s)}_{k}$ and $\hat{\Psi}^{(s)}_{\mu}$ versus time $\hat{t}$. (*c*) Temporal gradient of KE and its (*e*) budget versus time $\hat{t}$. (*d*) Temporal gradient of GPE and its (*f*) budget versus time $\hat{t}$.

4.3. *Numerical experiments*

Following Trewhela (2024), we resolved numerically the coupled, nonlinear partial differential equation system in (4.5*a*,*b*) using the method of lines. This numerical scheme is unconditionally stable and considered a constant pressure distribution $p = p_0$, so its robustness is not compromised by the ill-posed $\mu(I)$-rheology, even though it is regularised in (4.2). A total of 18 simulations were run, considering first a set of parameters $\mu_0 \times R_d = \{0.5, 0.8\} \times \{1.25, 1.5, 1.75, 2.0, 2.25, 2.5\}$ yielding 12 simulations to understand mid-range values, and second the set $\{0.4, 1.2, 1.6\} \times \{1.25, 2.5\}$ to explore extreme values for μ_0.

From the parameters introduced in table 1, the size ratio R_d and frictional coefficient μ_0 are the most determinants for segregation dynamics. The $\mu(I)$-rheology defining parameters are also relevant. Still, these are material dependent and altogether compile a large set of parameters that are particular for a type of grain. It is then hard to vary each parameter separately while extracting relevant information for segregation, and it is also at risk of exponentially increasing the number of simulations. Next, the empirical constants from the Trewhela *et al.* (2021*a*) scaling law and Utter &

Behringer (2004) need further validation in other flow configurations and particles, yet these have delivered consistent results against experimental and numerical data (Maguire *et al.* 2024; Singh, Liu & Henann 2024). For completion, Trewhela (2024) analysed the relevance of the parameters at the wall imposing shear, namely p_0, u_0 and μ_0 in this work. These parameters control the time scales at which segregation operates, but only μ_0 determines the segregation–diffusion balance or the resulting concentration ϕ_s profiles. Also, Trewhela (2024, figure 5) shows that R_μ does not have a determinant role in the segregation–diffusion balance, hence the resultant small-particle distribution ϕ_s, only on the velocity profiles $\hat{u}$. Thus we propose a brief but comprehensive set of simulations to shed light on the energetics under various frictional regimes and a wide range of segregation–mixing dynamics. Figure 1 illustrates an example of the spatiotemporal evolution of small-particle concentration $\phi_s(\hat{t}, \hat{z})$ and vertical profiles of the shear-driven granular flow $\hat{u}(\hat{t}, \hat{z})$, which are utilised to compute the energetics in (4.6) and (4.7).

Figure 2(*a*) shows time series of the segregation energy flux $\hat{\Psi}^{(s)}_{gps}$ and the diffusive energy flux $\hat{\Psi}^{(s)}_{k}$ for the frictional coefficient $\mu_0 = 0.8$ and a range of size ratio values $1.25 \leq R_d \leq 2.5$. The energy flux $\hat{\Psi}^{(s)}_{gps}$ is always negative, i.e. segregation continuously consumes the available GPE that the small particles have. Yet $\hat{\Psi}^{(s)}_{gps}$ exhibits two striking phases. The first phase is characterised by an exponential-like increase of the segregation flux, supported by the diffusive flux $\hat{\Psi}^{(s)}_{gpd}$ that also consumes GPE during this phase. The second phase is characterised by a change in the diffusive flux direction, which starts to raise the GPE until the granular flow balances into $\mathrm{d}\hat{E}^{(s)}_{gp}/\mathrm{d}\hat{t} \to 0$. This final state equilibrium is shown in figure 2(*c*), which illustrates $\mathrm{d}\hat{E}^{(s)}_{gp}/\mathrm{d}\hat{t}$ versus time. Figure 2(*b*) shows time series of the KE production due to shear taken by the small particles $\hat{\Sigma}^{(s)}_{k}$ and the KE dissipation rate owing to friction $\hat{\Psi}^{(s)}_{\mu}$. The magnitude of KE energetics is larger than the GPE energetics, showing that the system is dominated by particle–particle interactions with a short-lived transient phase, in which shear production at the boundary $\hat{\Sigma}^{(s)}_{k}$ is slightly higher than friction dissipation $\hat{\Psi}^{(s)}_{\mu}$. This results in the KE reaching a shear friction equilibrium significantly faster than the GPE equilibrium, which is hindered due to the slow pace segregation and the counter effect of diffusive remixing, as shown in figure 2(*d*). At the equilibrium state, the KE injected by shear is utilised to mobilise grains horizontally and maintain the bidisperse granular material fully or partially segregated across the sheared layer h. Such a balanced state – and therefore its GPE – should strongly depend on the competition between segregation and diffusion fluxes, which fosters mixing within the granular bulk.

The temporal evolutions of the bulk GPE and KE are shown in figures 2(*e*,*f*). These two plots confirm and aggregate the observations made from the overall energetics and their rates in figures 2(*a–d*). Much of the variation in $\hat{E}^{(s)}_{gp}$ comes from segregation that decreases the small particles' energy as a result of the onset of the kinetic sieving mechanism. Naturally, this decrease comes to a halt when it is balanced with diffusion, as observed in figure 2(*a*). The behaviour of the KE $\hat{E}^{(s)}_{k}$ is different, showing a strong and immediate increment due to the upper plate transferring momentum to the small particles located at the top. After the momentum is transferred through the whole bulk, the transient velocity profile is achieved, producing a plateau in $\hat{E}^{(s)}_{k}$. Finally, the KE plateau value is then modified by the segregation and diffusion balancing out into a steady state that varies with μ_0 and R_d. Notably, the plateau values for $\hat{E}^{(s)}_{k}$ show higher KE values for larger R_d values, which is consistent with the notion that larger particles result in larger inertia. This

trend is inverted after segregation and diffusion balance, with smaller R_d values having more KE. The latter shows the influence of diffusion and the effect of partially averaged quantities.

4.4. *Non-dimensional parameters and scalings*

From the numerical solutions (figures 1*b*,*c*) and the results shown in figure 2, the roles of segregation, diffusion and friction (or dissipation) are evident in the energetics distribution and balance. Besides the energy injection $\hat{\Sigma}_k^{(s)}$, the other three energetics represent well-defined processes that control the bidisperse granular flow dynamics. When combining and balancing these three main energetics, several non-dimensional parameters arise. A first quantity appears when analysing the GPE energetics: the competition between segregation $\Psi_{gps}^{(s)}$ and diffusion $\Psi_{gpd}^{(s)}$ is controlled by the segregation Péclet number

$$Pe = \frac{hf_{sl}}{\mathcal{D}_{sl}}, \tag{4.8}$$

which directly compares the segregation velocity f_{sl} to the particles' diffusion velocity scale $\mathcal{D}_{sl}/h$ (Gray & Chugunov 2006; Wiederseiner *et al.* 2011; Gray 2018), with h the thickness of the active sheared layer, which depends on the boundary condition parameters μ_0 and p_0 (see (4.4)). Yet in terms of the physical forcing of our system, it appears naturally that two other non-dimensional quantities balance the energetics. The second non-dimensional parameter, the Schmidt number $Sc = \mathcal{D}_{sl}/\nu_g$, balances particle diffusivity $\mathcal{D}_{sl}$ ($\Psi_{gpd}^{(s)}$) and momentum diffusion ($\Psi_{\mu}^{(s)}$), represented by the granular kinematic viscosity ν_g. This viscosity is defined as $\nu_g = \mu p/(\rho\dot{\gamma})$ when the Coulombic relation $\tau = \mu p$ combines with the equivalent Newtonian description $\tau = \eta_g\dot{\gamma}$ for the granular flow. Thus the remaining combination from the main three energetics is that of a balance between segregation $\Psi_{gps}^{(s)}$ and momentum diffusion or frictional dissipation $\Psi_{\mu}^{(s)}$. This balance results in the segregation–rheology Péclet number, which can be interpreted alternatively as a segregation Reynolds number and can be obtained as a combination of the other two non-dimensional numbers (Trewhela 2024):

$$Pe_{sr} = \frac{Pe}{Sc} = \frac{hf_{sl}}{\nu_g}. \tag{4.9}$$

The competition between segregation and frictional dissipation is condensed by the segregation–rheology Péclet number Pe_{sr}, which in our numerical experiments spans $Pe_{sr} = Pe/Sc \in [0.4, 300]$. For the specific case study, the granular kinematic viscosity ν_g is introduced following Trewhela (2024, (3.5)), which depends on size ratio R_d via the shear rate $\dot{\gamma}$. This results in a segregation–rheology Péclet number that can be defined and computed as

$$Pe_{sr} = \frac{I^2}{\Phi_P\hat{\mu}_0}\,\mathcal{F}(R_d,\phi_s) = \frac{\rho_* gh}{p_0}\,\frac{\rho_*\dot{\gamma}^2\bar{d}^2}{\mu_0 p_0}\,\mathcal{B}(R_d-1)(1+\mathcal{E}(R_d+1)(1-\phi_s)), \tag{4.10}$$

where $\Phi_P = \rho_* gh/p_0$ is a non-dimensional pressure that can also be interpreted as a solids volume fraction, and $\hat{\mu}_0$ is a χ_μ-dependent frictional coefficient that approximates to μ_0 when $\chi_\mu \to 0$, in our numerical solutions.

However, as emphasised earlier, Péclet numbers do not provide explicit information about the energy state of granular flows. To understand how segregation, mixing and

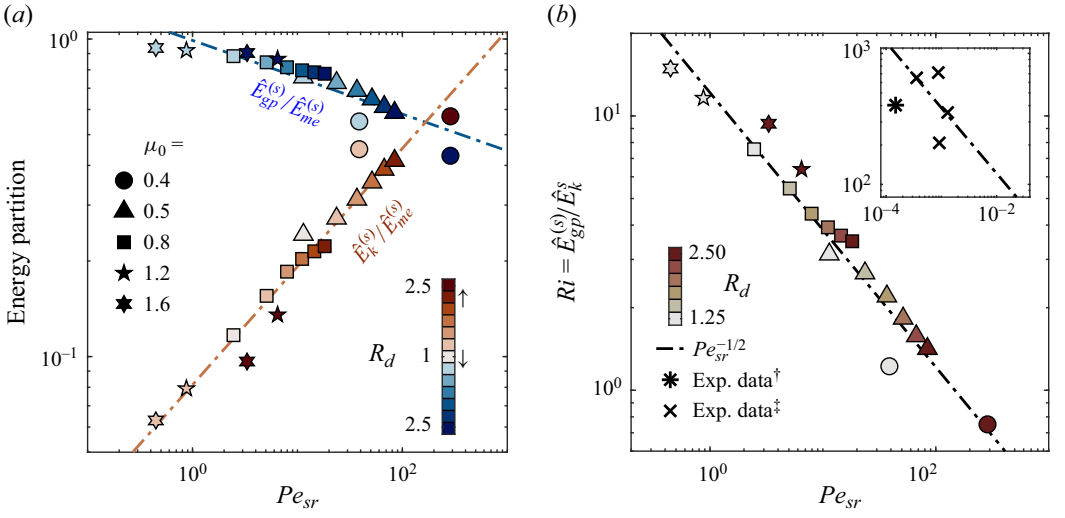

Figure 3. Results for all 18 numerical solutions. (*a*) Mechanical energy partition versus the segregation–rheology Péclet number Pe_{sr}. Reddish markers denote $\hat{E}_k^{(s)}/\hat{E}_{me}^{(s)}$, blueish markers denote $\hat{E}_{gp}^{(s)}/\hat{E}_{me}^{(s)}$, with $\hat{E}_{me}^{(s)} = \hat{E}_k^{(s)} + \hat{E}_{gp}^{(s)}$. (*b*) Ratio of the mechanical energy components, i.e. the Richardson number Ri versus Pe_{sr}. The inset shows experimental data of †van der Vaart *et al.* (2015) and ‡Wiederseiner *et al.* (2011) compared to the proposed scaling $Ri \sim Pe_{sr}^{-1/2}$.

dissipation dynamics affect the energy partition between GPE and KE, we can borrow the Richardson number Ri definition for stratified flows, weighting the balance between buoyancy and inertia (e.g. Caulfield 2021). Estimating Ri *a priori* is challenging, which leads us to explore a potential link between Ri and Pe_{sr} directly from our numerical experiments.

To unravel the relation between Pe_{sr} and Ri, we first examine the partition of the mechanical energy components (of the small-particle species) versus the segregation–rheology Péclet number. Figure 3(*a*) shows $\hat{E}_{gp}^{(s)}/\hat{E}_{me}^{(s)}$ (blue) and $\hat{E}_{k}^{(s)}/\hat{E}_{me}^{(s)}$ (red) versus Pe_{sr}, with $\hat{E}_{me}^{(s)} = \hat{E}_k^{(s)} + \hat{E}_{gp}^{(s)}$ the mechanical energy. For low Pe_{sr} ($\lesssim 10$), the KE is substantially smaller than the GPE, whereas for high Pe_{sr} ($\gtrsim 10^2$), the KE scales with or surpasses the GPE. From these results, we therefore expect the segregation–mixing state to be sensible to the energy partition, and in particular to the ratio between GPE and KE, here termed as the bulk Richardson number Ri of the granular flow:

$$Ri \equiv \frac{\hat{E}_{gp}^{(s)}}{\hat{E}_k^{(s)}} = \frac{gh}{u_0^2/2}\,\frac{\displaystyle\int_0^1 \phi_s \hat{z}\,\mathrm{d}\hat{z}}{\displaystyle\int_0^1 \hat{u}^2\,\mathrm{d}\hat{z}}. \tag{4.11}$$

This specific Ri is defined for small particles, but is extensible for other particle species.

Figure 3(*b*) plots Ri versus Pe_{sr} for our numerical solutions and experimental data from the literature. For the latter, we used the results from a 50 : 50 mixed shear cell experiment of van der Vaart *et al.* (2015), and the chute flow experiments of Wiederseiner *et al.* (2011). These studies provide measurements of the resulting small-particle distribution ϕ_s at steady-state conditions, which is key to determining the energy partition, hence the

ratio between GPE and KE. We determined the small particle concentration ϕ_s profiles of Wiederseiner *et al.* (2011) using their reported segregation rates q, diffusion coefficients D, and flow heights h (for their runs 22–25), and we directly used their flume slope (equivalent to μ_0 in steady state), particle density and shear rates to calculate the granular viscosity ν_g. Hence with their reported Péclet numbers Pe, we could obtain $Pe_{sr} = Pe/(\nu_g/D)$. For the van der Vaart *et al.* (2015) experiment, we computed Pe at the middle of their shear cell $\hat{z} = 1/2$ – in similar fashion to Trewhela *et al.* (2021*a*) – as Pe varies with depth $\hat{z}$ in such an experimental configuration. While a range of Pe values could be used, the balance between segregation and diffusion is most relevant at the small–large particle interface, which is precisely at $\hat{z} = 1/2$ in their experiment.

The results of this numerical and experimental dataset exhibit the distinct scaling relationship $Ri \propto Pe_{sr}^{-1/2}$ for six decades of Pe_{sr}, a direct result from a linear regression of the plot in logarithmic scale (dash-dotted line in figure 3*b*). Intriguingly, the empirical scaling law for Ri–Pe_{sr} does not seem straightforward to justify theoretically. However, a possible explanation for this scaling law relies upon the relationship between the active shear layer h – where the mechanical energy is stored and transformed – and the segregation–rheology Péclet and bulk Richardson numbers. Following the definitions in (4.10) and (4.4) yields that $Pe_{sr} \propto h^{-2}$. At the same time, the relation $Ri \propto h$ is retrieved directly from the bulk Richardson number definition. Therefore, combining both relationships, one may derive that $Ri \propto Pe_{sr}^{-1/2}$. Remarkably, this scaling shows excellent agreement with our compiled numerical results and experimental data from the literature (see the inset of figure 3*b*). Despite the fact that these experiments inherently have dispersion in their measurements, which we could not quantify from the reported data, the proposed scaling proves to be consistent as a follow-up to our numerical results. From this scaling, the energy partition of the granular flow can be readily predicted since Pe_{sr} is determined from prescribed system parameters in most cases, as our calculations from previous experiments demonstrate.

4.5. *Degree of mixing (and segregation)*

Yet how does the energy partition relate to the segregation–mixing state? We investigate this question through the 'degree of mixing'

$$\mathscr{M}_\phi = 1 - (\sigma_\phi/\sigma_{sg})^2, \tag{4.12}$$

with $\sigma_{sg}^2 = 1/2$ the variance of the fully segregated state of the species concentration ϕ_s, and σ_ϕ^2 the variance of ϕ_s. Thus $\mathscr{M}_\phi = 0$ denotes a perfectly segregated state, and $\mathscr{M}_\phi = 1$ a perfectly mixed state. It is apparent that the 'degree of segregation' in the system can be quantified from the reciprocal $\mathscr{S}_\phi = 1 - \mathscr{M}_\phi$. To explore first how the degree of mixing evolves in time throughout our numerical solutions, we plot $\mathscr{M}_\phi$ for five different cases in figure 4(*a*). The selected cases cover the whole range of friction coefficients μ_0 and size ratios R_d, and they result in differing mixing degrees $\mathscr{M}_\phi$ at steady state. These results show that all solutions pass by an intermediate, yet maximum, apparent mixing state, independently of whether the steady-state solution is mixed or segregated. Interestingly, the moment when this apparent mixing state happens is not the same for all cases. It appears to be controlled by diffusion, based on the results shown in figure 2(*a*). We plot in figure 4(*b*) the degree of mixing as a function of time for the experimental data of van der Vaart *et al.* (2015) against an equivalent numerical solution of their 50 : 50 mix experiment. Despite the evident point-to-point differences, numerical and experimental results show

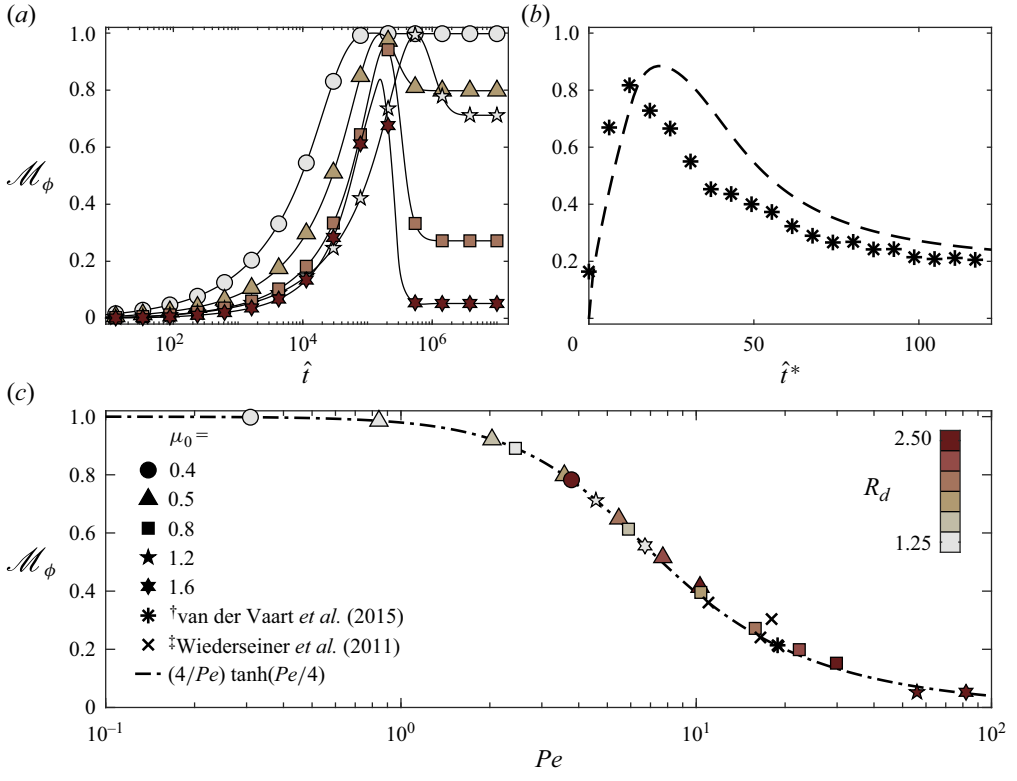

Figure 4. (*a*) Degree of mixing $\mathscr{M}_\phi$ as a function of time $\hat{t}$ for a subset of our numerical simulations. (*b*) A comparison between the degree of mixing $\mathscr{M}_\phi$ in the 50 : 50 mix experiment of van der Vaart *et al.* (2015) and its corresponding numerical solution, both as a function of the van der Vaart *et al.* (2015) non-dimensional time $\hat{t}^*$, which depends on their shear cell oscillation period. (*c*) Degree of mixing $\mathscr{M}_\phi$ at steady state as a function of the Péclet number Pe for our numerical simulations. Experimental data from †van der Vaart *et al.* (2015) and ‡Wiederseiner *et al.* (2011) are also included and plotted by considering their depth-averaged small-particle concentration. The whole dataset is compared to the here introduced theoretical expression $\mathscr{M}_\phi = (4/Pe)\tanh(Pe/4)$.

remarkable agreement – in magnitude and trend – both passing by the apparent mixing state, with the difference in $\mathscr{M}_\phi$ closing out at steady state. Notice that the evolution of the degree of mixing $\mathscr{M}_\phi$ in figure 4(*b*) differs from that observed in figure 4(*a*); this is because in the shear cell experiment, the onset of the shear rate is almost immediate compared to the shear flow studied here, which requires momentum to be transferred first.

Finally, to focus on the segregation–mixing state attained by the system, we examine $\mathscr{M}_\phi$ in terms of the segregation Péclet number Pe instead of Pe_{sr}. This allows us to isolate the mechanisms controlling mass distribution and GPE, excluding the friction needed to account for KE. Figure 4(*c*) shows $\mathscr{M}_\phi$ versus Pe. The results show that Pe strongly controls the degree of mixing, characterised by a nonlinear yet monotonic relationship. Within our parameter space, the maximum mixing state is attained at $Pe \approx 1$, with $\mathscr{M}_\phi \approx 0.99$. Conversely, the minimum mixing state, $\mathscr{M}_\phi \approx 0.05$, is achieved at $Pe \approx 10^2$, indicating the onset of a saturation state. Statistically, we expect $\mathscr{M}_\phi$ not to be zero at high Pe values as the transition region between small and large particles experiences a persistent remixing–segregation process, as seen in laboratory and numerical experiments

(e.g. Golick & Daniels 2009; van der Vaart *et al.* 2015; Ferdowsi *et al.* 2017; Singh & Henann 2024).

The nonlinear relationship between the degree of mixing and the segregation Péclet number can be derived theoretically from the steady-state solution for ϕ_s. From the segregation–diffusion equation in (4.5*a*,*b*), ϕ_s can be integrated to yield

$$\phi_s = \frac{\mathrm{e}^{Pe\,(\mathcal{K}-\hat{z})}}{1+\mathrm{e}^{Pe\,(\mathcal{K}-\hat{z})}}, \tag{4.13}$$

which is analogue to the solutions of Trewhela (2024, (3.3)), Wiederseiner *et al.* (2011, (11)) and Gray & Chugunov (2006, (3.4)). The integration constant $\mathcal{K}$ corresponds to the depth-averaged concentration, i.e. $\overline{\phi_s} = 0.5$ for the studied case, and variable for the Wiederseiner *et al.* (2011) experiments. With this analytical solution for ϕ_s, its variance can be expressed as $\sigma_\phi^2 = \mathbb{E}(\phi_s^2) - \mathbb{E}(\phi_s)^2$, where $\mathbb{E}(\cdot)$ denotes the expected value. The theoretical calculation of σ_ϕ^2 alongside the value $\sigma_{sg} = 1/2$ yields an analytical expression for the degree of mixing:

$$\mathscr{M}_\phi = -\frac{4}{Pe}\left(\frac{1-\mathrm{e}^{Pe/2}}{1+\mathrm{e}^{Pe/2}}\right) = \frac{4}{Pe}\tanh\left(\frac{Pe}{4}\right). \tag{4.14}$$

Reciprocally, the latter expression provides an explicit function for the degree of segregation as a function of the Péclet number for segregation:

$$\mathscr{S}_\phi = 1 - \mathscr{M}_\phi = 1 - \frac{4}{Pe}\tanh\left(\frac{Pe}{4}\right), \tag{4.15}$$

where Pe for a first-order approximation in $R_d - 1$ is a function of the empirical constants $\mathcal{A}$ (Utter & Behringer 2004) and $\mathcal{B}$ (Trewhela *et al.* 2021*a*) corresponding to $Pe = \mathcal{B}(R_d - 1)\rho g h/(\mathcal{A}p_0)$.

In figure 4(*c*), our compiled dataset of numerical solutions and experimental data from van der Vaart *et al.* (2015) and Wiederseiner *et al.* (2011) shows excellent agreement with the proposed theoretical curve in (4.14) (dash-dotted line), which indicates that mixing (and segregated) states depend solely on Pe, hence on the parameters that define it. The latter provides a general relationship that does not depend on flow configuration or scale, a fact inherited from the variable conditions considered in our shear flow case, and the shear cell and chute flow configurations from the previous experimental results included here.

5. Concluding remarks

This paper introduces a continuum framework for the energetics of particle-size segregation in granular flows, providing general analytical expressions for the energetics governing the mechanical energy budget in the system. The framework builds upon the convective–diffusion equation (Gray 2018) for segregation and a recent segregation scaling law (Trewhela *et al.* 2021*a*), enabling the study of the complex physics of bidisperse granular flows from a mechanical energy perspective. The proposed approach is easily extensible to polydisperse systems, and does not depend on a particular rheological model, local or non-local, as long as the stress tensor is properly described.

We illustrate the framework's applicability by studying the energetics and mechanical energy partition in shear-driven bidisperse granular flows alongside the partially regularised $\mu(I)$-rheology (Barker & Gray 2017). Numerical solutions exploring different friction coefficients μ_0 and particle-size ratios R_d reveal: (i) the existence of distinctive

phases in the segregation–mixing energy pathways, heavily marked by segregation and diffusive remixing; and (ii) that the bulk Richardson number, defined as the ratio between GPE and KE at equilibrium, follows the scaling relationship $Ri \equiv \hat{E}_{gp}^{(s)}/\hat{E}_{k}^{(s)} \propto Pe_{sr}^{-1/2} = (Sc/Pe)^{1/2}$, for $10^{-4} \leq Pe_{sr} \leq 300$, with Pe_{sr} the segregation–rheology Péclet number, and Pe and Sc the segregation Péclet number and Schmidt number, respectively. Furthermore, we derived a theoretical expression for the degree of mixing $\mathscr{M}_\phi$ (and segregation $\mathscr{S}_\phi = 1 - \mathscr{M}_\phi$), which depends only on Pe; our numerical simulations and laboratory experiments from the literature (Wiederseiner *et al.* 2011; van der Vaart *et al.* 2015) validate this theoretical result. Our findings hint that the energy partition of bidisperse granular flows can be predicted from the Péclet and Schmidt numbers, providing a powerful tool for understanding and controlling segregation–mixing states in granular flows across various engineering applications and geophysical systems.

Acknowledgements. H.N.U. was supported by the University of Pennsylvania start-up grant. We thank the Visiting Professor Grant 2024 granted by the Universidad Adolfo Ibañez, which allowed this work to be developed in person. We are also grateful for the constructive feedback provided by three referees. In particular, we thank one of the anonymous referees, whose insights allowed us to offer a potential explanation for the relationship between the bulk Richardson number and the segregation–rheology Péclet number. The colour maps used in this paper's figures are suitable for both colour-vision deficient and colour-blind readers (Crameri 2018). Finally, we especially thank Olivia Trewhela and Helia Ulloa – the authors' respective newborn daughters – for making the process of writing this paper more joyful.

Funding. T.T. received support from Agencia Nacional de Investigación y Desarrollo (ANID) through FONDECYT Iniciación Project 11240630.

Declaration of interests. The authors report no conflict of interest.

Author ORCIDs.
Tomás Trewhela https://orcid.org/0000-0002-7461-8570;
Hugo N. Ulloa https://orcid.org/0000-0002-1995-6630.

References

Barker, T. & Gray, J.M.N.T. 2017 Partial regularisation of the incompressible $\mu(I)$-rheology for granular flow. *J. Fluid Mech.* **828**, 5–32.

Caulfield, C.P. 2021 Layering, instabilities, and mixing in turbulent stratified flows. *Annu. Rev. Fluid Mech.* **53** (1), 113–145.

Chassagne, R., Frey, P., Maurin, R. & Chauchat, J. 2020 Mobility of bidisperse mixtures during bedload transport. *Phys. Rev. Fluids* **5** (11), 114307.

Crameri, F. 2018 Scientific colour maps. Zenodo. Available at http://doi.org/10.5281/zenodo.1243862.

Fan, Y., Schlick, C.P., Umbanhowar, P.B., Ottino, J.M. & Lueptow, R.M. 2014 Modelling size segregation of granular materials: the roles of segregation, advection and diffusion. *J. Fluid Mech.* **741**, 252–279.

Ferdowsi, B., Ortiz, C.P., Houssais, M. & Jerolmack, D.J. 2017 River-bed armouring as a granular segregation phenomenon. *Nat. Commun.* **8**, 1363.

Fry, A.M., Umbanhowar, P.B., Ottino, J.M. & Lueptow, R.M. 2018 Effect of pressure on segregation in granular shear flows. *Phys. Rev.* E **97**, 062906.

Gajjar, P. & Gray, J.M.N.T. 2014 Asymmetric flux models for particle-size segregation in granular avalanches. *J. Fluid Mech.* **757**, 297–329.

GDR MiDi 2004 On dense granular flows. *Eur. Phys. J.* E **14** (4), 341–365.

Golick, L.A. & Daniels, K.E. 2009 Mixing and segregation rates in sheared granular materials. *Phys. Rev.* E **80**, 042301.

Gray, J.M.N.T. 2018 Particle segregation in dense granular flows. *Annu. Rev. Fluid Mech.* **50** (1), 407–433.

Gray, J.M.N.T. & Chugunov, V.A. 2006 Particle-size segregation and diffusive remixing in shallow granular avalanches. *J. Fluid Mech.* **569**, 365–398.

HURLEY, R.C. & ANDRADE, J.E. 2015 Friction in inertial granular flows: competition between dilation and grain-scale dissipation rates. *Granul. Matter* **17** (3), 287–295.

JHA, B., CUETO-FELGUEROSO, L. & JUANES, R. 2011 Fluid mixing from viscous fingering. *Phys. Rev. Lett.* **106** (19), 194502.

JIANG, Y.-J., FAN, X.-Y., LI, T.-H. & XIAO, S.-Y. 2018 Influence of particle-size segregation on the impact of dry granular flow. *Powder Technol.* **340**, 39–51.

JOHN SOUNDAR JEROME, J. & DI PIERRO, B. 2018 A note on Stokes' problem in dense granular media using the $\mu(I)$-rheology. *J. Fluid Mech.* **847**, 365–385.

JOP, P., FORTERRE, Y. & POULIQUEN, O. 2006 A constitutive law for dense granular flows. *Nature* **441** (7094), 727–730.

KAMRIN, K., HILL, K.M., GOLDMAN, D.I. & ANDRADE, J.E. 2024 Advances in modeling dense granular media. *Annu. Rev. Fluid Mech.* **56**, 215–240.

MAGUIRE, E.S.F., BARKER, T., RAUTER, M., JOHNSON, C.G. & GRAY, J.M.N.T. 2024 Particle-size segregation patterns in a partially filled triangular rotating drum. *J. Fluid Mech.* **979**, A40.

OTTINO, J.M. & KHAKHAR, D.V. 2000 Mixing and segregation of granular materials. *Annu. Rev. Fluid Mech.* **32** (1), 55–91.

PEREIRA, G.G. & CLEARY, P.W. 2017 Segregation due to particle shape of a granular mixture in a slowly rotating tumbler. *Granul. Matter* **19** (2), 23.

SINGH, H. & HENANN, D.L. 2024 Anti-plane segregation and diffusion in dense, bidisperse granular shear flow. *Phys. Rev. Fluids* **9** (9), 094301.

SINGH, H., LIU, D. & HENANN, D.L. 2024 Continuum modelling of size segregation and flow in dense, bidisperse granular media: accounting for segregation driven by both pressure gradients and shear-strain-rate gradients. *J. Fluid Mech.* **988**, A43.

SUN, Q., JIN, F. & ZHOU, G.G.D. 2013 Energy characteristics of simple shear granular flows. *Granul. Matter* **15** (1), 119–128.

THORNTON, A., WEINHART, T., LUDING, S. & BOKHOVE, O. 2012 Modeling of particle size segregation: calibration using the discrete particle method. *Intl J. Mod. Phys.* C **23**, 1240014.

TREWHELA, T. 2024 Segregation–rheology feedback in bidisperse granular flows: a coupled Stokes' problem. *J. Fluid Mech.* **983**, A45.

TREWHELA, T., ANCEY, C. & GRAY, J.M.N.T. 2021*a* An experimental scaling law for particle-size segregation in dense granular flows. *J. Fluid Mech.* **916**, A55.

TREWHELA, T., GRAY, J.M.N.T. & ANCEY, C. 2021*b* Large particle segregation in two-dimensional sheared granular flows. *Phys. Rev. Fluids* **6**, 054302.

TRIPATHI, A., KUMAR, A., NEMA, M. & KHAKHAR, D.V. 2021 Theory for size segregation in flowing granular mixtures based on computation of forces on a single large particle. *Phys. Rev.* E **103**, L031301.

ULLOA, H.N. & LETELIER, J.A. 2022 Energetics and mixing of thermally driven flows in Hele-Shaw cells. *J. Fluid Mech.* **930**, A16.

UMBANHOWAR, P.B., LUEPTOW, R.M. & OTTINO, J.M. 2019 Modeling segregation in granular flows. *Annu. Rev. Chem. Biomol. Engng* **10**, 129–153.

UTTER, B. & BEHRINGER, R.P. 2004 Self-diffusion in dense granular shear flows. *Phys. Rev.* E **69**, 031308.

VAN DER VAART, K., GAJJAR, P., EPELY-CHAUVIN, G., ANDREINI, N., GRAY, J.M.N.T. & ANCEY, C. 2015 Underlying asymmetry within particle size segregation. *Phys. Rev. Lett.* **114**, 238001.

VARELA-ROSALES, N.R., SANTAROSSA, A., ENGEL, M. & PÖSCHEL, T. 2023 Granular binary mixtures improve energy dissipation efficiency of granular dampers. *Granul. Matter* **25** (3), 49.

WIEDERSEINER, S., ANDREINI, N., ÉPELY-CHAUVIN, G., MOSER, G., MONNEREAU, M., Gray, J.M.N.T. & Ancey, C. 2011 Experimental investigation into segregating granular flows down chutes. *Phys. Fluids* **23** (1), 013301.